

**PARAMETRIC STUDY OF MICROCHANNEL
SUBSTRATES FOR HIGH POWER LED
APPLICATIONS**

**DHEEPAN CHAKRAVARTHII
MUSIRI KANAGARAJ**

UNIVERSITI SAINS MALAYSIA

2019

**PARAMETRIC STUDY OF MICROCHANNEL
SUBSTRATES FOR HIGH POWER LED
APPLICATIONS**

by

**DHEEPAN CHAKRAVARTHII
MUSIRI KANAGARAJ**

**Thesis submitted in fulfillment of the requirements
for the degree of
Doctor of Philosophy**

August 2019

ACKNOWLEDGEMENT

First and foremost, I express my deep gratitude to my supervisor, Associate Professor. Dr. Mutharasu Devarajan, for his guidance, encouragement and support during the entire course of this study. His powerful and insightful thinking, productive discussions and constructive comments in research meetings had not only been instrumental in the realization of this work but will also help enormously in my future endeavours. I would like to thank Dr. Shanmugan Subramani for his support throughout this study.

I would like to express my gratitude to Institute of Post-Graduate Studies (IPS), USM for funding me throughout this research by USM Fellowship which relieved me of financial insecurity.

The success of this work has been made possible through the support of many individuals who encouraged me throughout my research here at University of Science, Malaysia (USM). I would like to thank all the colleagues, interns and project students, especially to Ms. Norazlina and Mr. Lim Wei Qiang of Thermal Management Research Laboratory (TMRL), School of Physics, USM for their provoking conversations, questions and suggestions which excelled me in one or the other way.

Finally, I would like to thank my family: my mother who supported me to the core without which this dissertation would have been just imaginary, my father showering from the heavens and my ever-friendly brother who shouldered me in tough times.

DHEEPAN CHAKRAVARTHII M K

TABLE OF CONTENTS

ACKNOWLEDGEMENT	ii
TABLE OF CONTENTS	iii
LIST OF TABLES	x
LIST OF FIGURES	xi
LIST OF SYMBOLS	xvii
LIST OF ABBREVIATIONS	xxi
ABSTRAK	xxiii
ABSTRACT	xxv
CHAPTER 1 – INTRODUCTION	1
1.1 Introduction to thermal management in electronics cooling	1
1.2 Thermal management in LEDs	2
1.3 Introduction to microchannel heat sinks	3
1.4 Problem statement	3
1.5 Objectives	4
1.6 Research Contribution	5
1.7 Thesis outline	5
CHAPTER 2 – LITERATURE REVIEW	8
2.1 Overview	8
2.2 Light Emitting Diodes (LEDs)	8
2.3 Thermal management of LEDs	11
2.3.1 Heat Sinks	12
2.3.2 Heat pipes	13
2.3.3 Microchannel heat sinks	14

2.4	Selection of microchannel.....	17
2.4.1	Microchannel with different cross-sections	17
2.4.1(a)	Rectangular microchannels	18
2.4.1(b)	Circular microchannels	20
2.4.1(c)	Triangular microchannels	21
2.4.1(d)	Trapezoidal microchannels	22
2.4.1(e)	Non-circular microchannels	23
2.4.1(f)	Microchannel with unique cross-sections	23
2.4.1(g)	Inference	28
2.4.2	Microchannel with different geometry.....	31
2.4.2(a)	Curved microchannels	31
2.4.2(b)	Wavy microchannels	32
2.4.2(c)	Serpentine microchannels	33
2.4.2(d)	Convergent-divergent microchannels	34
2.4.2(e)	Converging or Diverging microchannels	35
2.4.2(f)	Microchannel with unique wall geometry.....	36
2.4.2(g)	Inference	41
2.4.3	Employable microchannel.....	43
2.5	Thermal Transient characterization.....	44
2.5.1	Theoretical background.....	44
2.5.1(a)	Thermal resistance and junction temperature	47
2.5.2	Thermal and optical relation in thermal measurements	48
2.6	Summary	49

CHAPTER 3 – METHODOLOGY	51
3.1 Outline.....	51
3.2 Computational Fluid Dynamics	52
3.2.1 Computational domain.....	52
3.2.2 Assumptions and boundary conditions	54
3.2.3 Solution method	55
3.2.4 Mesh sensitivity analysis	56
3.2.5 Numerical Validation	57
3.3 Parametric analysis.....	59
3.3.1 Geometrical parameters	59
3.3.1(a) Effect of variation in entry and exit length.....	60
3.3.1(b) Effect of converge-diverge angle	62
3.3.1(c) Effect of hydraulic diameter	62
3.3.1(d) Effect of aspect ratio.....	63
3.3.1(e) Effect of solid-fluid thickness ratio	64
3.3.1(f) Effect of solid-fluid thermal conductivity ratio	64
3.3.2 Operational parameters	64
3.3.2(a) Effect of mass flow rate	64
3.3.2(b) Effect of heat input	65
3.4 Fabrication of prototypes	65
3.4.1 Choice of channel geometry.....	65
3.4.2 Test section fabrication	65
3.5 Surface topography analysis	66
3.6 Thermal transient characterization.....	67
3.6.1 Device Under Test (DUT).....	68

3.6.2	<i>K</i> -factor calibration	70
3.6.3	Experimental setup with Julabo	71
3.6.4	Optical measurements	72
3.6.5	Still air chamber test for different cooling conditions	73
	3.6.5(a) Natural convection.....	74
	3.6.5(a) Forced convection.....	74
3.7	Velocity measurement in Microchannel	75
3.7.1	Fluid Reservoirs	76
3.7.2	Linear actuator	77
3.7.3	Syringe	77
3.7.4	DC power supply	78
3.7.5	DC speed controller.....	78
3.7.6	Microchannel test section.....	79
3.8	Experimental test procedure.....	80
3.8.1	Degassing procedure	80
3.8.2	Experimental steps	80
3.8.3	Uncertainties	81
3.8.4	Data Reduction.....	81
3.9	Chapter summary	83
	CHAPTER 4 – NUMERICAL RESULTS AND DISCUSSION.....	84
4.1	Overview	84
4.2	Surface contours.....	84
4.2.1	Pressure drop.....	84
4.2.2	Temperature distribution.....	86
4.2.3	Flow trajectories.....	87

4.3	Preliminary examination	89
4.3.1	CD microchannels	89
4.3.2	DC microchannels	97
4.4	Numerical results for parametric analysis	103
4.4.1	Influence of channel length	103
4.4.1(a)	CD microchannel	103
4.4.1(b)	DC microchannel	105
4.4.2	Influence of converge-diverge angle	107
4.4.2(a)	CD microchannel	107
4.4.2(b)	DC microchannel	109
4.4.3	Influence of hydraulic diameter	112
4.4.3(a)	CD microchannel	113
4.4.3(b)	DC microchannel	115
4.4.4	Influence of aspect ratio	117
4.4.4(a)	CD microchannel	118
4.4.4(b)	DC microchannel	119
4.4.5	Influence of solid-fluid thickness ratio	122
4.4.5(a)	CD microchannel	122
4.4.5(b)	DC microchannel	125
4.4.6	Influence of solid-fluid thermal conductivity ratio	127
4.4.7	Summary of numerical analysis	128
4.5	Effect of operational parameters	129
4.5.1	Effect of mass flow rate	129
4.5.2	Effect of heat flux	130
4.6	Fabrication of CD and DC channelled substrates	131

4.7	Chapter summary	135
CHAPTER 5 – THERMAL TRANSIENT RESULTS AND DISCUSSION		136
5.1	Overview	136
5.2	Preliminary experiments using Julabo system	136
5.2.1	Influence of input current.....	137
5.2.1(a)	Thermal resistance	137
5.2.1(b)	Junction temperature	143
5.2.2	Influence of ambient temperature	145
5.2.2(a)	Thermal resistance	145
5.2.2(b)	Junction temperature	148
5.2.3	Influence of converge-diverge angle.....	150
5.2.3(a)	Thermal transient analysis	150
5.2.3(b)	Optical analysis	154
5.2.3(c)	Summary.....	156
5.3	Influence of different cooling conditions.....	156
5.3.1	Natural convection	157
5.3.2	Forced convection	162
5.4	Time-constant spectrum characterization	167
5.4.1	Natural convection	168
5.4.2	Forced convection	172
5.5	Comparison of optical performance.....	173
5.6	Chapter summary	176
CHAPTER 6 – FLUID FLOW CHARACTERISTICS.....		177
6.1	Overview	177
6.2	Fluid flow characteristics	177

6.3	Comparison of Experimental and Numerical data	182
6.4	Chapter summary	185
CHAPTER 7 – CONCLUSIONS AND RECOMMENDATIONS		186
7.1	Conclusions	186
7.2	Recommendations for future work.....	188
REFERENCES		189
APPENDICES		
LIST OF PUBLICATIONS		

LIST OF TABLES

		Page
Table 2.1	Summary of review on investigations in microchannels with different cross-section	25
Table 2.2	Summary of review on investigations in microchannels with different wall geometries	38
Table 3.1	Grid independence	57
Table 3.2	Geometrical parameters	60
Table 3.3	Specification of SMD LED at ambient temperature of 25°C	69
Table 3.4	Specifications of CAHB-10 Linear actuator	77
Table 3.5	Specifications of Syringe used	77
Table 3.6	Specifications of DC power supply	78
Table 3.7	Specifications of DC speed controller	79
Table 3.8	Uncertainty in experimental measurements	81
Table 4.1	Surface roughness of fabricated substrates	133
Table 5.1	Variation of T_j and R_{th} with different T_a	150
Table 5.2	T_j (°C) for different substrates with Natural Convection	162
Table 5.3	T_j (°C) for different substrates with Forced Convection	166
Table 5.4	CRI for LEDs mounted on different substrates	175
Table 5.5	Wavelength of light emitted from LEDs mounted on different Substrates	176

LIST OF FIGURES

		Page
Figure 2.1	LED lighting principle (a) The energy band diagram of a PN junction without any bias, (b) Light emission occurs when electrons and holes recombine	9
Figure 2.2	(a) Direct bandgap and (b) indirect bandgap	10
Figure 2.3	Structure of LED	10
Figure 2.4	(a) Horizontal plate fin heat sink (b) Radial heat sink with pin fins (c) Heat sink with perforations	12
Figure 2.5	LED mounted on cooling system using flat heat pipe	14
Figure 2.6	Parallel microchannel with different cross-sections (a) rectangular, (b) circular, (c) triangular, (d) trapezoidal, (e) elliptical, (f) parabolic and (g) V-shaped	18
Figure 2.7	(a) Heat transfer performance correlations for Microchannels with different cross-sectional geometry, (b) Pressure drop and friction factor correlations for Microchannels with different cross-sectional geometry	28
Figure 2.8	Microchannels with different wall geometries: (a) parallel, (b) curved, (c) wavy, (d) serpentine, (e) converging-diverging, (f) diverging/converging	31
Figure 2.9	Thermo-hydraulic performance correlations for Microchannels with different wall geometry, (a) Nusselt number and (b) Pressure drop	41
Figure 2.10	Schematic Measurement setup of thermal transient	45
Figure 2.11	Simulated cooling transient of a thermal model with temperature change vs assumed time-constants	47
Figure 3.1	Methodology	51
Figure 3.2	Computational domain	52
Figure 3.3	Assumptions and boundary conditions in FloEFD 16	53
Figure 3.4	Data plots calculated for (a) Centreline velocity and (b) Shear stress	56

Figure 3.5	Meshing grid level in FloEFD	56
Figure 3.6	Nusselt number correlation for validation of numerical results	59
Figure 3.7	2D CAD model of microchannel segments, (a) CD channel showing segments 1, 2, 3, 4 and 5 (b) DC channel showing segments 1, 2, 3, 4 and 5	59
Figure 3.8	Variation of L_1 to L_5 for constant converge-diverge angle for (a) CD microchannel (b) DC microchannel	61
Figure 3.9	Variation of L_1 to L_5 for different converge-diverge angle for (a) CD microchannel (b) DC microchannel	63
Figure 3.10	Micro-milling cutter	66
Figure 3.11	Bruker's Dimension Edge Atomic Force Microscope	67
Figure 3.12	(a) Device Under Test (DUT) (b) Resistive network for DUT (c) Dimensions of DUT	68
Figure 3.13	K -factor calibration curve of LED	70
Figure 3.14	Thermal transient experimental setup (a) Schematic diagram (b) Experimental picture	71
Figure 3.15	LED package and substrate setup mounted on the cold plate	72
Figure 3.16	MK350N Plus Handheld Spectrometer	73
Figure 3.17	Experimental setup for optical measurement	73
Figure 3.18	Natural convection experiment with still air chamber and DUT	74
Figure 3.19	DUT for forced convection experiments	74
Figure 3.20	Forced convection experiment with still air chamber and DUT	75
Figure 3.21	(a) Schematic layout of experimental flow loop and (b) Hydrodynamic test setup	76
Figure 3.22	Microchannel test section	79
Figure 4.1	Pressure drop contours in (a) CD microchannel (b) 3mm parallel microchannel (c) DC microchannel (d) 0.5mm parallel microchannel	85
Figure 4.2	Surface temperature distribution in substrates with (a) CD microchannel (b) 3mm parallel microchannel (c) DC microchannel (d) 0.5mm parallel microchannel	87

Figure 4.3	Flow trajectories in (a) CD microchannel (b) 3mm parallel microchannel (c) DC microchannel (d) 0.5mm parallel microchannel	88
Figure 4.4	Vector plots for fluid flow in (a) CD microchannel (b) 3mm parallel microchannel (c) DC microchannel (d) 0.5mm parallel microchannel	89
Figure 4.5	Surface temperature distribution of CD substrates with (a) 10° (b) 45° (c) 60° and (d) 90°	90
Figure 4.6	Vector plots in CD channels with (a) 10° (b) 45° (c) 60° and (d) 90°	91
Figure 4.7	Flow trajectories in CD channels with (a) 10° (b) 45° (c) 60° and (d) 90°	92
Figure 4.8	Pressure contours in CD channels with (a) 10° (b) 45° (c) 60° and (d) 90°	94
Figure 4.9	Variation of (a) Pressure (b) Velocity along the axial distance of different CD microchannels	95
Figure 4.10	Variation of wall shear stress along the axial distance of different CD microchannels	96
Figure 4.11	Surface temperature distribution of DC substrates with (a) 10° (b) 45° (c) 60° and (d) 90°	97
Figure 4.12	Vector plots in DC channels with (a) 10° (b) 45° (c) 60° and (d) 90°	98
Figure 4.13	Flow trajectories in DC channels with (a) 10° (b) 45° (c) 60° and (d) 90°	99
Figure 4.14	Pressure contours in DC channels with (a) 10° (b) 45° (c) 60° and (d) 90°	100
Figure 4.15	Variation of (a) Pressure (b) Velocity along the axial distance of different DC microchannels	101
Figure 4.16	Variation of wall shear stress along the axial distance of different DC microchannels	102
Figure 4.17	Variation of surface temperature in CD microchannels with different L_I at (a) $D_h=651\mu\text{m}$ and (b) $D_h=512\mu\text{m}$	104
Figure 4.18	Flow trajectories in CD channel with $L_I=9\text{mm}$	105

Figure 4.19	Variation of surface temperature in DC microchannels with different L_I at (a) $D_h=651\mu\text{m}$ and (b) $D_h=512\mu\text{m}$	106
Figure 4.20	Flow trajectories in DC channels with $L_I=3.25\text{mm}$	107
Figure 4.21	Flow trajectories in CD channels with (a) 20° , (b) 30° , (c) 40° , (d) 45° , (e) 50° , (f) 60° , (g) 70° , (h) 80° and (i) 90°	109
Figure 4.22	Flow trajectories in DC channels with (a) 10° , (b) 20° , (c) 30° , (d) 40° , (e) 45° , (f) 50° , (g) 60° , (h) 70° , (i) 80° and (j) 90°	112
Figure 4.23	Variation of (a) Surface temperature & pressure drop, and (b) Shear stress & velocity in CD microchannels with different D_h	113
Figure 4.24	Flow trajectories in CD channels with D_h of (a) $189\mu\text{m}$, (b) $359\mu\text{m}$, (c) $512\mu\text{m}$ and (d) $651\mu\text{m}$	115
Figure 4.25	Variation of (a) Surface temperature & pressure drop, and (c) Shear stress & velocity in DC microchannels with different D_h	115
Figure 4.26	Flow trajectories in DC channels with D_h of (a) $189\mu\text{m}$, (b) $359\mu\text{m}$, (c) $512\mu\text{m}$ and (d) $651\mu\text{m}$	116
Figure 4.27	Variation of (a) Surface temperature & pressure drop, and (b) Shear stress & velocity in CD microchannels with different aspect ratio	118
Figure 4.28	Flow trajectories in CD channels with W_{max} of (a) 1, (b) 1.5, (c) 2, (d) 2.5 and (e) 3 mm	119
Figure 4.29	Variation of (a) Surface temperature & pressure drop, and (b) Shear stress & velocity in DC microchannels with different aspect ratio	120
Figure 4.30	Flow trajectories in DC channels with W_{max} of (a) 1, (b) 1.5, (c) 2, (d) 2.5 and (e) 3 mm	121
Figure 4.31	Variation of (a) Surface temperature & pressure drop, and (b) Shear stress & velocity in CD microchannels with different solid to fluid thickness ratio	122
Figure 4.32	Surface temperature distribution in CD channels with t_s/t_f of (a) 0.6, (b) 0.8, (c) 1, (d) 1.2 (e) 1.4, (f) 1.6, (g) 1.8 and (h) 2	124
Figure 4.33	Variation of (a) Surface temperature & pressure drop, and (d) Shear stress & velocity in DC microchannels with different solid to fluid thickness ratio	125

Figure 4.34	Surface temperature distribution in DC channels with t_s/t_f of (a) 0.6, (b) 0.8, (c) 1, (d) 1.2 (e) 1.4, (f) 1.6, (g) 1.8 and (h) 2	126
Figure 4.35	Variation of surface temperature in CD and DC microchannels with different solid to fluid thermal conductivity ratio	127
Figure 4.36	Summary of numerical analysis for CD microchannels	128
Figure 4.37	Summary of numerical analysis for DC microchannels	128
Figure 4.38	Variation of surface temperature for different inlet mass flow rate in (a) CD microchannel and (b) DC microchannel	129
Figure 4.39	Variation of surface temperature for different input heat flux in (a) CD microchannel and (b) DC microchannel	131
Figure 4.40	Different substrates (a) Bare Al (b) PII-0.5mm (c) PII-3mm (d) CD20 (e) CD45 (f) CD60 (g) CD90 (h) DC45 (i) DC60 (j) DC90 and (k) CD20 with ruler	132
Figure 5.1	Differential structure functions of LED at input current (a) 300mA (c) 500mA (d) 700mA	139
Figure 5.2	Cumulative structure functions of LED at input current (a) 300mA (b) 500mA (c) 700mA	141
Figure 5.3	Smoothed response curves of LED at input current (a) 300mA (b) 500mA (c) 700mA	144
Figure 5.4	Differential structure functions of LED at different ambient temperatures (a) 25°C (b) 35°C (c) 45°C (d) 55°C	146
Figure 5.5	Cumulative structure functions of LED at different ambient temperatures (a) 25°C (b) 35°C (c) 45°C (d) 55°C	147
Figure 5.6	Smoothed response curves of LED at different ambient temperatures (a) 25°C (b) 35°C (c) 45°C (d) 55°C	149
Figure 5.7	Differential structure functions of different (a) CD substrates (b) DC substrates	151
Figure 5.8	Smoothed response Curve for bare, CD and DC substrates	153
Figure 5.9	Optical performance of LEDs	155
Figure 5.10	Differential structure functions of LED with natural convection at input current (a) 300mA (b) 500mA (c) 700mA	159

Figure 5.11	Smoothed response curves of LED with natural convection at input current (a) 300mA (b) 500mA (c) 700mA	161
Figure 5.12	Differential structure functions of LED with forced convection at input current (a) 300mA (b) 500mA (c) 700mA	163
Figure 5.13	Smoothed response curves of LED with forced convection at input current (a) 300mA (b) 500mA (c) 700mA	165
Figure 5.14	Time constant intensity of LED with natural convection at (a) 300mA (b) 500mA (c) 700mA	169
Figure 5.15	Time constant intensity of LED with forced convection at (a) 300mA (b) 500mA (c) 700mA	171
Figure 5.16	Comparison of optical parameters of LED (a) CCT (b) LUX	174
Figure 6.1	Time taken by the fluid to flow through various channels for Different PWM output	178
Figure 6.2	Velocity calculated from experiment in different microchannels	179
Figure 6.3	Comparison of velocity calculated from experiment and simulation in different microchannels	182

LIST OF SYMBOLS

$a(t)$	Total step-function response at time t
$a(Z)$	Simplest step-function response
A_c	Area of heat conduction path
A_s	Total surface area of the substrate
A_{ws}	Wetted surface area of the channel
c	Speed of light
C_p	Specific heat capacity
C_{Σ}	Cumulative thermal capacitance
De	Dean number
D_h	Hydraulic diameter
E	Luminous efficacy
E_0	Rated efficacy at rated temperature T_o
f	Friction factor
f_p	Specific frequency of photons
g	Acceleration due to gravity
G_k	Perturbation energy production
h_{avg}	Average heat transfer coefficient
h_{out}	Heat carried away by the channel
h_{pl}	Planck's constant
H_c	Height of the channel
I_{in}	Input current
I_s	Sensor current
I_{tot}	Total current
k_e	Relative reduction rate of efficacy

K	K -factor
K_f	Fluid thermal conductivity
K_s	Solid thermal conductivity
K_λ	Thermal conductivity coefficient
L_n	Length of the n^{th} segment ($n = 1,2,3,4$ and 5)
L_r	Characteristic length of channel
Nu_{exp}	Nu calculated from the experiments
Nu_{model}	Nu calculated from theoretical correlations' model
P	Pressure
P_{dis}	Dissipated power
P_{el}	Electrical input power
P_o	Poiseuille number ($f.Re$)
P_{opt}	Optical output power
Pr	Prandtl number
$P_{thermal/off}$	Thermal power when LED is OFF
$P_{thermal/on}$	Thermal power when LED is ON
q_{loss}	Heat loss
Q_{in}	Input heat
Ra	Rayleigh number
Re	Reynolds number
R_i	Resistance at i^{th} magnitude
R_{th}	Thermal Resistance
R_{thja}	Total thermal resistance
R_{thjs}	Partial R_{th} of LED
R_{th-die}	Partial R_{th} of die

$R_{th-die-lead}$	Partial R_{th} of die to lead-frame
$R_{th-lead-sp}$	Partial R_{th} of lead-frame to solder-pad
R_{th-tp}	Partial R_{th} of thermal pad
R_{th-sub}	Partial R_{th} of substrate
R_{Σ}	Cumulative thermal resistance
t	time
t_s	thickness of the substrate
T	Temperature
T_a	Ambient temperature
T_f	Average fluid temperature
T_{fi}	Inlet fluid temperature
T_{fo}	Outlet fluid temperature
T_j	Junction temperature
T_{ref}	Reference temperature
T_s	Average surface temperature of substrate
T_{si}	Inlet surface temperature
T_{so}	Outlet surface temperature
U_{avg}	Average streamline velocity
V	Voltage
V_f	Forward voltage
W_{avg}	Average width of the channel
W_g	Bandgap energy
W_{max}	Larger width of the channel
W_{min}	Smaller width of the channel
α	Thermal diffusivity of the fluid

σ_ε	Turbulence energy loss
σ_k	Effective Prandtl number for turbulence energy
ρ	Density of the fluid
β	Thermal expansion coefficient
ΔT	Maximum temperature difference of package and ambient
ΔT_a	Change in T_a
ΔT_{ja}	Temperature rise
ΔV_f	Change in V_f
ε	Rate of dissipation of turbulence energy
κ	Turbulence kinetic energy
\dot{m}	mass flow rate
θ_{CD}	Converging-diverging angle
θ_{DC}	Diverging-converging angle
τ_i	Time constant at i^{th} magnitude
μ	Dynamic viscosity of the fluid
μ_t	Perturbation viscosity
ν	Kinematic viscosity of the fluid
γ	Aspect ratio
λ	Wavelength of light emitted by LED
λ_p	Wavelength of photon

LIST OF ABBREVIATIONS

AFM	Atomic Force Microscope
Al	Aluminium
AlN	Aluminium Nitride
CCT	Correlated Colour Temperature
CD	Converging-diverging
CFD	Computational Fluid Dynamics
CRI	Colour Rendering Index
Cu	Copper
DC	Diverging-converging
DI	Deionized
DPC	Direct Plated Copper
DUTs	Devices Under Test
FHCS	Flat head cap screw
FHP	Flat heat pipe
Ga	Gallium
GaN	Gallium Nitride
IC	Integrated Circuit
Kn	Knudsen number
JEDEC	Joint Electron Device Engineering Council
LED	Light Emitting Diode
LEE	Light Emitting Efficiency
LUX	Luminous Flux per unit area
MCHS	Micro-Channel Heat Sink
MOSFET	Metal Oxide Semiconductor Field Effect Transistor

MQW	Multiple Quantum Well
MCPCBs	Metal Core Printed Circuit Boards
Nu	Nusselt number
PCBs	Printed Circuit Boards
PDMS	Poly Dimethyl Siloxane
Po	Poiseuille number
RC	Resistor-Capacitor
Re	Reynolds number
RTDs	Resistance Temperature Detectors
RSM	Response Surface Methodology
SAC	Still Air Chamber
SMD	Surface-mount Device
TDP	Thermal Design Power
TSP	Temperature Sensitive Parameter
T3ster	Thermal Transient Tester
TIM	Thermal Interface Material
UV	Ultra-Violet
VF	Volume Fraction
MAE	Mean Average Error

KAJIAN PARAMETER TERHADAP SUBSTRAT SALURAN MIKRO UNTUK APLIKASI LED KUASA TINGGI

ABSTRAK

Dalam kajian ini, keratan rentas substrat saluran-mikro yang tidak seragam telah dikaji bagi pengurusan haba dalam LED. Pencirian telah dipanjangkan ke numerik dan eksperimen bagi mencapai substrat saluran yang baharu untuk aplikasi LED yang berkuasa tinggi. Daripada kajian literatur yang menyeluruh, saluran menumpu-mencapah dan saluran mencapah-menumpu telah fokus untuk penyelidikan ini kerana terdapat beberapa kelebihan seperti pembentukan aliran sekunder yang cekap dan pengurangan pendidihan nukleus. Kajian parametrik secara terperinci dan konstruktif telah dijalankan menggunakan simulasi CFD untuk mengenal pasti prestasi terma substrat berdasarkan parameter geometri yang berbeza seperti panjang saluran, sudut-sudut tumpu-capah, garis pusat hidraulik (D_h) dan nisbah aspek (γ). Pembentukan aliran sekunder yang unggul dalam saluran-mikro CD20 ($L_l=9\text{mm}$, $D_h=512\mu\text{m}$, $\gamma=3\text{mm}$) dan DC90 ($L_l=3.25\text{mm}$, $D_h=651\mu\text{m}$, $\gamma=3\text{mm}$) telah menyumbang kepada peningkatan dalam prestasi pemindahan haba.—Daripada keputusan simulasi berangka, saluran CD20 dan DC90 telah menunjukkan prestasi nasa yang tinggi. Substrat saluran CD dan DC telah dihasilkan melalui proses permilan mikro dan kekasaran permukaan telah diukur menggunakan AFM. LED berkuasa tinggi dipasang pada CD dan DC substrat yang berbeza dan pencirian nasa tidak tetap telah dilakukan menggunakan Penguji Transien Terma (T3Ster[®]). Parameter terma yang kritikal seperti rintangan terma dan suhu simpang telah dikira daripada fungsi struktur dan lengkung tindak balas lancar. Pengaruh arus masuk dan suhu persekitaran ke atas substrat CD dan DC telah dijelaskan bagi memastikan konsistensi dalam prestasi terma tanpa mengira keadaan operasinya. Spektrum pemalar masa telah

memberikan pemahaman yang lebih besar mengenai sumbangan saluran CD dan DC dalam meningkatkan pelepasan haba. Bukti menunjukkan rintangan haba untuk substrat CD20 dan DC90 pada arus masuk yang tinggi adalah lebih rendah daripada substrat yang terdedah sebanyak 6.84% dan 16.54% masing-masing . Selain itu, suhu persimpangan berkurangan dengan ketara sebanyak 2.68 °C dan 3.68 °C bagi mengakui prestasi haba substrat yang telah dicadangkan. Ia perlu diperhatikan bahawa substrat DC mempunyai keupayaan pelepasan haba yang lebih tinggi dalam perolakan semulajadi (7.45%) dan keadaan penyejukan pemanasan terpaksa (64.62%) dengan udara sebagai cecair kerja. Fakta ini telah disokong oleh prestasi optik LED yang telah dipertingkatkan seperti fluks bercahaya, Suhu Warna Korelasi, Indeks Rendering Warna dan panjang gelombang. Oleh itu, penyesuaian teknik penyejukan mungkin bergantung kepada keadaan operasi LED. Eksperimen pemindahan fasa tunggal telah dijalankan dengan air sebagai cairan kerja bagi menyiasat prestasi thermo-hidraulik CD dan saluran DC yang telah dicadangkan. Aliran bendalir dan parameter pemindahan haba seperti penurunan tekanan, faktor geseran, nombor Poiseuille, pekali pemindahan haba dan nombor Nusselt diukur dan dikira menggunakan persamaan tradisional. Peranan daya geseran yang disertai oleh tekanan dan daya inersia dikaji dengan keputusan eksperimen. Saluran DC mempunyai prestasi pemindahan haba yang lebih tinggi dengan penalti penurunan tekanan yang dapat dikurangkan dengan penyelidikan yang selanjutnya. Keputusan eksperimen yang diperhatikan telah dikaitkan dengan hasil kajian sedia ada untuk kesimpulan selanjutnya.

PARAMETRIC STUDY OF MICROCHANNEL SUBSTRATES FOR HIGH POWER LED APPLICATIONS

ABSTRACT

In this study, microchannel substrates with non-uniform cross-sections were investigated for thermal management in LEDs. Extensive characterizations were done numerically and experimentally for high power LED applications to employ the novel substrates with channels. From the comprehensive literature review, converging-diverging and diverging-converging channels were focussed for this research due to certain advantages such as efficient secondary flow formation and mitigation of nucleation boiling. A detailed and constructive parametric study was conducted by CFD simulations to identify the thermal performance of substrates based on different geometrical parameters such as channel length, converge-diverge angles, hydraulic diameters (D_h) and aspect ratio (γ). Ideal secondary flow formation in CD20 and DC90 microchannels contributed for enhanced heat transfer performance. From the numerical results, the substrates with higher thermal performance were CD20 ($L_I=9\text{mm}$, $D_h=512\mu\text{m}$, $W_{max}=3\text{mm}$) and DC90 ($L_I=3.25\text{mm}$, $D_h=651\mu\text{m}$, $W_{max}=3\text{mm}$). The CD and DC channelled substrates were manufactured by micro milling process and the surface roughness were measured using AFM. A high-power LED was mounted on different CD and DC substrates and thermal transient characterizations were done using Thermal Transient Tester (T3Ster[®]). The critical thermal parameters such as thermal resistance and junction temperature were calculated from the structure functions and smoothed response curves. The influence of input current and ambient temperature on CD and DC substrates were elaborated to affirm the consistency in the thermal performance irrespective of its operating conditions. Time-constant spectrums provided greater insights on contribution of CD and DC channels in improving the

heat dissipation. Evidently, the thermal resistance for CD20 and DC90 substrates at high input current were lower than the bare substrate by 7.86% and 16.54% respectively. Furthermore, the junction temperature decreased significantly by 2.68°C and 3.68°C which acknowledges the thermal performance of proposed substrates. It is noteworthy that the DC substrates possess the ability of higher heat dissipation in both the natural convection (7.45%) and forced convection (64.62%) cooling conditions with air as the working fluid. These facts were supported by enhanced optical performance of LEDs such as luminous flux, Correlated Colour Temperature, Colour Rendering Index and wavelength. Hence, an adaptive cooling technique is possible depending on the LEDs operating conditions. Experiments were conducted with water as the working fluid to investigate the velocity of fluid flow through proposed CD and DC channels. At a mean flow rate, the velocity of CD20 was higher by 42.1% and that of DC90 was lower by 55.4% than their equivalent parallel microchannel. The role of viscous forces in the channels of varying aspect ratio contributed for difference in velocity of fluid flow. The observed experimental results were validated with the numerical predictions. The maximum deviation between experimental and numerical data was 14.82% which was in acceptable limits. The consistency in numerical results against the experimental measurements suggests the feasibility of the numerical simulations.

CHAPTER 1

INTRODUCTION

1.1 Introduction to thermal management in electronics cooling

With the advancements in aerospace technology, microelectromechanical systems, lighting systems, hybrid data centres and microfluidics, the miniature size electronic chips in such applications are the need of the century. According to the Moore's law, the increase in operating temperature of the electronic boards results in deterioration of component's durability. Compact microelectronic designs have led to miniaturization of device and as a result, high power density occurs in electronic boards. The microelectronics and power electronics industries faces the challenge of handling high heat flux ranging from 30 W/cm^2 to 110 W/cm^2 which is expected to rise to 300 W/cm^2 [1] [2]. Also, International Technology Roadmap for Semiconductors (ITRS, 2015) alarmed that the thermal management in high performance chip packages will be crucial for intermittent and efficient operation of the parent device. Over next few years, the failure rate in electronic components are estimated to increase drastically and thermal management in electronics will become a major bottleneck process for the development of microelectronics industry.

Conventional cooling systems fails to meet such high demand of high heat flux removal consistently. Innovative as well as effective thermal solution is demanded by the growing technical advancements. From economic perspective, the overall cost of the system depends on the selection of appropriate cooling system too. Above all, the maintenance of active cooling system incurs production cost and unexpected lay-offs. In modern electronics system, innovative cooling techniques with minimal

complications in intended application are expected by possible elimination of heat sinks.

1.2 Thermal Management in LEDs

Light Emitting Diode (LED) is a solid-state lighting device with high electricity to light conversion efficiency over incandescent light bulbs and fluorescent lamps [3]. The frightening energy demands and power consumption witnesses implementation of solid state lighting devices over traditional luminescent technologies. According to US National Lighting Bureau, the implementation of LEDs would increase by 74% in 2030 and thereby reducing the global power consumption by 46% [2]. Certain advantages such as high luminous flux, low-power consumption, robust operating range, eco-friendly and extended lifespan validates its employment. LEDs are widely used in automotive, backlighting, architectural, decorations and residential lighting applications. In addition, the LEDs are subjected to different ambient ranging from spacecrafts to deep marine water [4-6]. However, thermal management in LEDs are a major concern as the operational parameters should be maintained at optimum levels for reliable and everlasting performance [7, 8]. The light output from the LEDs decreases when it exceeds the critical junction temperature [9, 10]. Careful attention is mandatory as further increase in junction temperature leads to thermal runaway and eventual failure of the device. The heat flow path in lighting device can be estimated by calculating the thermal resistance (R_{th}) which is given by:

$$R_{th} = \frac{T_j - T_a}{TDP} \quad (1.1)$$

where T_j is the junction temperature of LED which is the maximum temperature measured at the heat source and T_a is the ambient temperature of operating conditions. Thermal Design Power (TDP) which is defined by the maximum amount of heat

dissipated by the component to operate at safe and reliable operating conditions. Incorporation of heat transfer enhancements such as heat spreader, thermal interface materials, heat sinks and other heat transfer mechanisms are designed to minimize the overall thermal resistance of the system or package.

1.3 Introduction to Microchannel Heat sinks

Though research are being conducted on different thermal heat dissipation techniques, microchannel heat sinks are very promising in terms of high heat flux dissipation capacity and compatibility with the electronics system. Heat transfer in microchannels takes place by efficient fluid transport at the channel walls. However, the performance of microchannel heat sinks is quite unsatisfactory due to high pumping power requirement, pressure/temperature fluctuations, reduced critical heat flux, flow reversal and thermal stresses. Lot of research are being carried out in improving the microchannel system. The term “microchannel” refers to the size of channel cross-section which is normally expressed in terms of hydraulic diameter (D_h). D_h is inversely related to the ratio of wetted surface area to the volume of the channel. However, the threshold criterion for transition from macro to microscale channels is still debatable where microchannels and minichannels are categorized with D_h between $10\mu\text{m}$ - $200\mu\text{m}$ and $200\mu\text{m}$ - 3mm respectively [11].

1.4 Problem Statement

Miniaturization of electronic devices increases the power density of the individual components for high speed processing of data. Adversely, the heat dissipation from the devices increases exponentially. Thermal management in electronics applications witnesses implementation of active and passive cooling techniques depending on the heat flux generated at the junction of the device. In case

of LED, the junction temperature remains a crucial factor as it is inversely proportional to the reliable performance and life span. The thermal resistance of the device and the system itself depends on the maintenance of the junction temperature at optimal levels. However, identification of suitable heat dissipation technique poses a major threat in terms of prompt temperature reduction, overall weight and cost of the system. Although passive cooling techniques are being implanted for LED lighting system, inability to perform during the breakdown remains a major concern. Furthermore, employment of active cooling system for lighting system arises a buzz pertaining to its applications. Innovative design accompanied with adaptive cooling techniques are demanded for efficient thermal management in LED applications.

1.5 Objectives

- i. To study the influence of different geometrical parameters on thermal performance of converging/diverging microchannel and identify optimum parameters
- ii. To investigate the thermal performance of LEDs mounted on channelled substrates by estimation of critical thermal parameters such as thermal resistance and junction temperature
- iii. To identify the effect of natural convection and forced convection conditions in channelled substrates on LED thermal performance
- iv. To analyse the influence of proposed substrates on optical performance of LEDs under different cooling conditions
- v. To evaluate the thermo-hydraulic parameters of proposed microchannels using single phase heat transfer experiments

1.6 Research Contribution

It is evident from the above discussion that the efficient cooling techniques are the need of the century. In LED applications, efforts are made to achieve thermal management using high heat dissipating substrates. Usually, the substrates are bulk material where heat conduction is the predominant mode of heat transfer. Design of substrate by increasing the surface area of heat transfer for additional convection heat transfer will lead to a conjugate heat transfer. Novel substrates with microchannels are proposed in this thesis for conjugate heat transfer mechanism where conduction and convection take place simultaneously. Conventional channels are not chosen as the heat transfer in the lighting system may saturate beyond certain cycle and the temperature profiles becomes almost uniform. Hence, channels with non-uniform cross-section are ideal choice for further implementation as the fluid transport to the channel walls increases the heat transfer. On selection of novel channels, the geometrical parameters should be analysed in detail as improper design can cause serious problems. To the best of author's knowledge, no studies were performed with channelled substrates as an option of LED applications. Further, cooling techniques with natural and forced convection in the channels and experimental validation of LED performance has been little explored previously. In this intention, an elaborate research with multi-functional microchannel substrates has been carried out which is disserted in forthcoming chapters.

1.7 Thesis Outline

Chapter 1 – Introduction: This chapter discussed the challenges in thermal management of LEDs and motivation for this research. Suitable alternatives and the need for adaptive cooling techniques were stressed. From the discussions, the problem statement and the research objectives were proposed.

Chapter 2 – Literature Review: A detailed literature review of publications from the studies on thermal management in electronics cooling and LEDs as follows:

1. To analyse the different cooling techniques used in heat dissipation of LEDs:
 - a. Passive cooling techniques – Heat sinks
 - b. Active cooling techniques – Heat pipes, Microchannel heat sinks
2. To choose microchannel heat sinks, appropriate selection criterion should be set. Hence, a detailed analysis was conducted on evolution of microchannels with:
 - a. Different cross-sections
 - b. Different wall geometry
3. Theoretical background in thermal transient characterization of semiconductor devices. Studies on determination of total thermal resistance of LEDs mounted on substrates by thermal transient testing.

Chapter 3 – Methodology: A detailed methodology to achieve the mentioned objectives is given in this chapter. Assumptions and boundary conditions for numerical simulations and selection of geometrical parameters by constructive design are elaborated. The experimental steps and procedure for thermal transient characterization is given. The experimental conditions for thermal measurements and optical measurements are described with schematic diagrams. Also, the experimental setup for natural convection and forced convection experiments are explained to clarify the differences. Further, experimental facility for heat transfer experiments are described, including the flow loop, test sections, equipment, experimental procedures and data reduction.

Chapter 4 – Results and Discussion – Numerical Results: This chapter presents the numerical results for all the cases of geometrical parameters and flow parameters

considered. Surface contours for pressure drop, temperature and flow trajectories within the channels are discussed. The optimum design with lower surface temperature is selected for further fabrication.

Chapter 5 – Results and Discussion – Thermal Transient Characterization:

Thermal transient results for selected substrates are explained in this chapter. The influence of channelled substrates on thermal performance of LEDs are analysed with the help of structure functions smoothed response functions and time-constant spectrums. The effect of different input current and ambient temperature on thermal parameters of the LEDs such as total thermal resistance and junction temperature are elaborated. The LEDs mounted on different substrates are subjected to different cooling conditions and its effect on heat dissipation are investigated. Furthermore, the optical analysis on LEDs proved the enhancement in the efficiency of light output.

Chapter 6 – Results and Discussion – Fluid flow characteristics: This chapter aims at determination of velocity fluid flow in proposed microchannel substrates with water as the working fluid. Velocity is measured from the experimental setup and compared with numerical results obtained as in Chapter 4. Suitable observations are drawn by calculating the deviation between experimental and numerical data.

Chapter 7 – Conclusion: The conclusions that can be drawn from this research is presented in final chapter. In addition, research recommendations drawn from this dissertation are enlisted as a means of future prospect.

CHAPTER 2

LITERATURE REVIEW

2.1 Overview

Thermal management in LEDs is a major challenge as the research community address different heat dissipation techniques. Active and passive cooling techniques are being carried out depending on the heat flux generated in particular applications. The studies and reports of researchers on different thermal management techniques are explored in this chapter. The focusses are:

- Thermal Management in LEDs
- Active and Passive cooling techniques
- Selection of Microchannels (cross-section and wall geometry)
- Performance evaluation by Thermal Transient characterization

2.2 Light Emitting Diodes (LEDs)

For high-power LED chips, the key part is the “p-n junction” where a quantum well or multiple quantum well (MQW) layers are sandwiched with a p-GaN layer and an n-GaN layer [12]. In a p-n junction, the “p” material contains an excess of positive charges (also called holes) due to the absence of electrons. The “n” material contains an excess of negative charges due to the presence of electrons. To understand the lighting principle, consider an unbiased p-n junction. Figure 2.1 shows the p-n energy band diagram. The depletion region extends mainly into the p-side. There is a potential barrier from E_c on the n-side to the E_c on the p-side, which is called the built-in voltage, V_0 . This potential barrier prevents the excess free electrons on the n-side from diffusing into the p-side. When a voltage V is applied to the junction, the built-in

potential is reduced from V_0 to $V_0 - V$. This allows electrons from the n-side to get injected into the p-side and recombine with the holes there, resulting in spontaneous emission of photons (light).

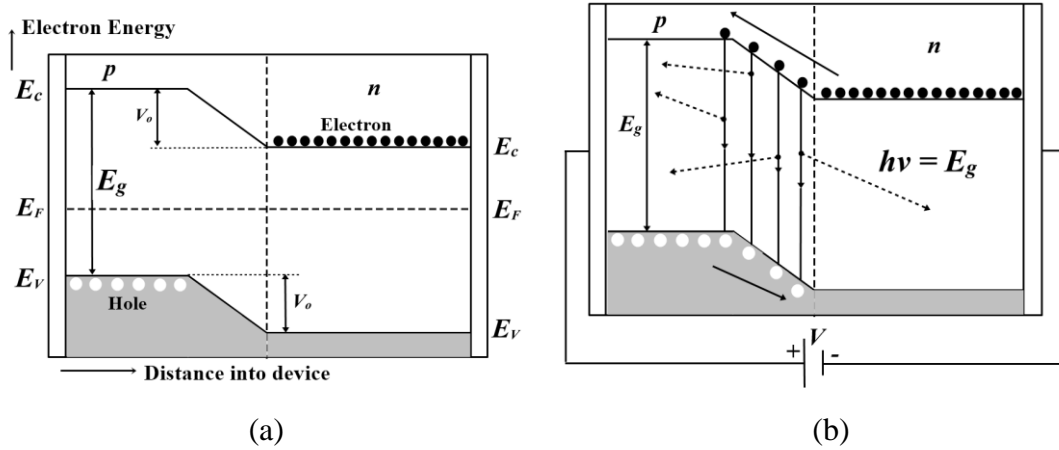


Figure 2.1: LED lighting principle. (a) The energy band diagram of a PN junction without any bias. (b) Light emission occurs when electrons and holes recombine [13]

Light from an LED is produced in the form of photons when excited electrons in the conduction band falls and recombines with a hole in the valence band through a direct energy state transition (direct band gap). The photons emitted have a specific frequency which is derived from Eq. (2.1):

$$f_p = \frac{W_g}{h_{pl}} \quad (2.1)$$

The wavelength of the photon can be obtained from Eq. (2.2):

$$\lambda_p = \frac{h_{pl} \cdot c}{W_g} \quad (2.2)$$

whereby the wavelength of the photon is λ_p , f is the frequency of the photon, W_g is the bandgap energy, c is the speed of light and h_{pl} is Planck's constant.

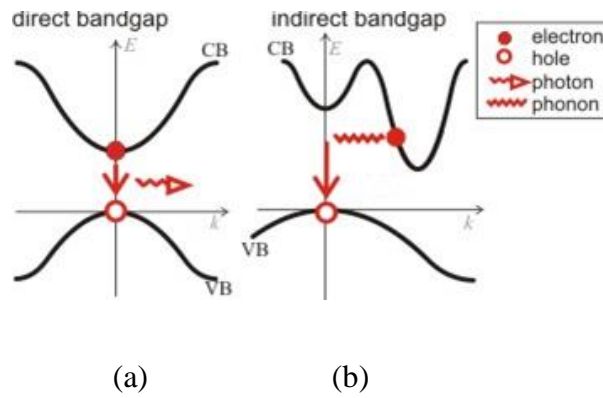


Figure 2.2: (a) Direct bandgap and (b) indirect bandgap [8]

This phenomenon only occurs in direct bandgap materials. Direct bandgap materials have an energy band structure such that the minimum energy level of the conduction band (non-localized electrons are free to move here) and the maximum energy level of the valence band (place where vacancies of excited electrons are situated) are placed in the same k -wavelength number as shown in Figure 2.2(a). This type of recombination process is called radiative recombination. In indirect bandgap materials as shown in Figure. 2.2(b), when the electron recombines with a hole, the energy is transferred to the vibration energy of the semiconductor lattice in the form of phonons, causing heat generation in the LED [14-16]. A simple structure of an LED is shown in Figure 2.3.

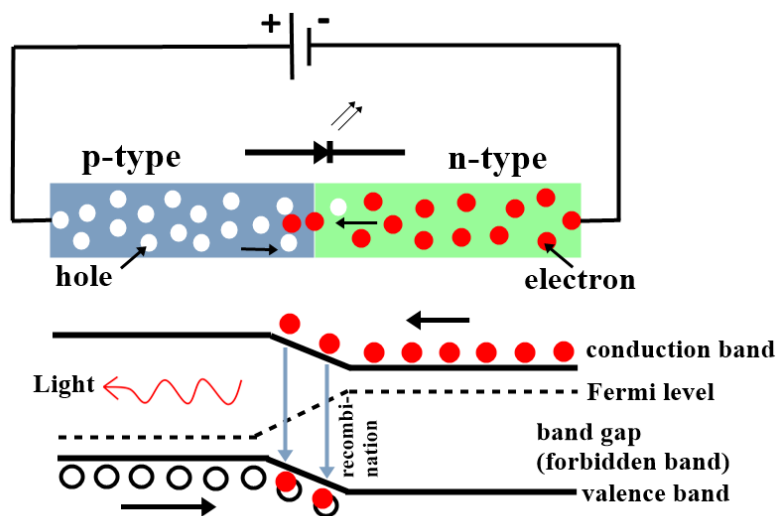


Figure 2.3: Structure of LED [16]

2.3 Thermal Management of LEDs

Advanced researches are being conducted to propose efficient heat transfer technology [17-21]. The heat generated at the junction of LEDs should be dissipated to ambient by providing appropriate heat transfer path [22]. In general, the principal mechanism for cooling LED is to transfer heat from LED junction to substrate and subsequently to the environment. Hence, numerous researches are focused on using suitable substrates to which the LEDs are attached. PCBs (Printed Circuit Boards) and MCPCBs (Metal Core Printed Circuit Boards) are commonly used substrates for LED applications. MCPCBs (Metal Core Printed Circuit Boards) are preferred over PCBs as substrates with base metal possess efficient heat dissipation capacity [18]. LED with ceramic packages offered higher thermomechanical stress due to high modulus of ceramic mold [23, 24]. However, LED mounting process with ceramic packages should be critical as it can lead to delaminating interface layers. Direct plated copper (DPC) substrates were also used proposed to increase the thermal performance of LEDs [25]. The influence of different thickness and thermal conductivity of Al substrates were examined by Yang *et al* [26]. The reduction in substrate thickness increases the thermal spreading resistance and chip temperature of LEDs.

Identification of suitable heat transfer path increases the heat dissipation from the junction of LEDs [27]. Progressive researches were carried out to modify the heat transfer path for higher thermal performance of LEDs. Enhanced thermal flow path should be accomplished by improving its thermal conductivity or heat dissipation capacity. Introduction of thermal vias, Thermal Interface Materials (TIMs) and conductive coating for heat transfer enhancement are other forms of improving the heat dissipation capacity of substrates [7, 18, 28-30]. Thermal conductivity of dielectric layers in the MCPCB were introduced to increase the thermal and optical

efficiency of low power SMD LEDs [31]. Novel substrates and heat sink designs were introduced for increased heat transfer coefficients [19, 32]. The heat dissipation efficiency in LED lamps was increased by introducing coated-ventilation holes in Multi-layered substrates [33]. Structures with copper filled thermal holes was fabricated on AlN ceramic substrates to increase the heat dissipation and thermal reliability of Deep Ultra-Violet (DUV) LEDs [34]. Parallel grooves were inscribed on sapphire substrate for improving the thermal performance of high power Ultra-Violet (UV) LEDs [35].

Passive and active cooling methods are prevalent choices in electronics cooling. Active cooling methods operates under forced convection while the passive cooling operates under natural convection phenomenon [36]. The choice of active or passive cooling methods depends on the heat flux generated by the heat source.

2.3.1 Heat Sinks

Heat sinks contribute to increased thermal conduction path from the junction of LEDs to ambient [40]. Numerous heat sinks designs were proposed to increase the heat dissipation in LED package as shown in Figure 2.4. For LED modules, heat sinks with extended surfaces are sensible cooling device which dissipates heat efficiently through natural convection.

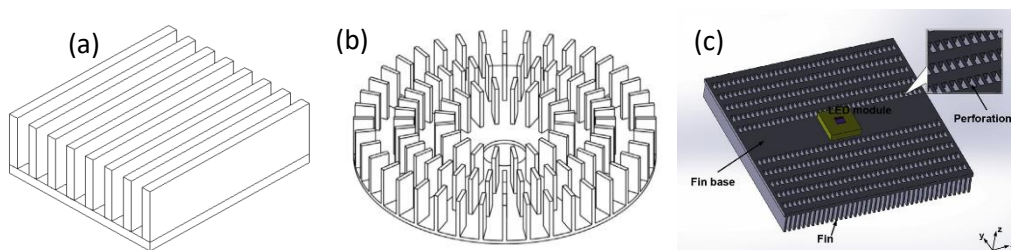


Figure 2.4: (a) Horizontal plate fin heat sink [37] (b) Radial heat sink with pin fins [38] (c) Heat sink with perforations [39]

Finned heat sinks are preferred as it possess a fin base and fins arises vertically from fin base to enhance the upward air flow as a result of buoyancy [36, 38, 41, 42]. The fin direction may be horizontal or vertical depending on the heat dissipation path from the heat source [37, 43]. The fin may be plate fin or pin fin type which depends on the material of the heat sink and the packaging methods [44]. The plate fin and pin fin heat sinks have been extensively studied in optimizing the length of fins, height of fins and thickness of the fin base [45-47]. In the previous studies reported by Huang *et al.*, Tseng *et al.* and Meng *et al.*, an opening was introduced in the heat sinks to enhance the circulation of air flow [48-51]. Tseng *et al.* increased the heat transfer in printed circuit board by 12% through induction of opening in fin base [49, 50]. Circular Perforations were also made on the fins to increase the heat transfer rate [51]. Min *et al.* incorporated the openings both in the fin base and in fins to improve the cooling performance in LEDs [39]. They reported 30.5% decrease in total thermal resistance of LEDs with 23.7% increase in luminous efficacy in comparison to conventional heat sink. Major drawback in implementation of heat sinks is its inability to remove high heat generated at the verge of system failure. The reliability of electronic components decreases by 5% and the life span reduces during heat accumulation in excess of 1°C nominal temperature [52]. Hence, effective cooling technology should be implemented to meet the demands of high heat generated by electronic components.

2.3.2 Heat Pipes

Different types of active cooling techniques were incorporated in electronics cooling systems [32, 53-57]. Efforts are being made to achieve maximum thermal performance using cooling techniques with reduced complexity to reduce the overall cost of the lighting system [58]. Heat pipes with miniature loops was first

demonstrated for electronic cooling applications by Yu *et al.* [59] and subsequently by Pastukhov *et al* [60]. Novel heat pipes were first introduced in LED array system and its influence on LED junction temperature were studied by calculating the thermal resistance of the system [53]. The start-up performance, temperature uniformity of flat heat pipe (FHP) heat sink (as shown in Figure. 2.5) and its thermal resistance were studied by Lu *et al* [61]. The evaluation of different filling rates and inclination angles of heat pipe aids in the application of LED cooling system. Through evolution, various parameters of heat pipes such as orientation, coolant, material of heat sink, ventilation fan, and fin shape and intervals were analysed for high heat dissipation performance [62, 63]. However, irregularities in heat transfer, limits in length and diameter of heat pipe, system design complexity, etc sets a major drawback in heat pipe implementations [63, 64].

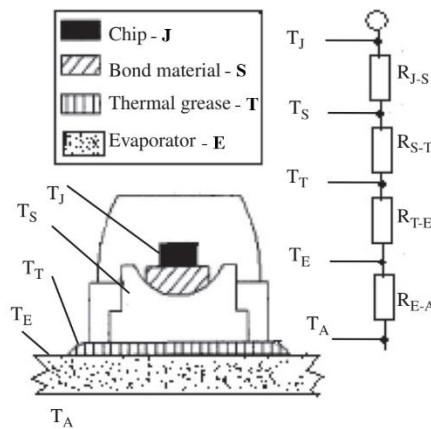


Figure 2.5: LED mounted on cooling system using flat heat pipe [61] (subset shows the thermal resistance model)

2.3.3 Microchannel heat sinks

Microchannel heat sinks (MCHS) draws major attention among researchers for past two decades due to its unique attributes such as high area-to-volume ratios, compactness, high heat flux dissipation capacity and smaller coolant inventory [65, 66]. Although the implementation of MCHS are common with electronic cooling

system where the heat generation is more than 30 W/cm^2 , only few researches were carried out for LED applications [67]. Based on the literature with heat flux as input, the implementation of MCHS for LED applications can be extensively studied as it remains unexplored.

The foundation for pioneering research on microchannels for engineering applications were began by Tuckerman and Pease [68]. Although a breakthrough was expected in the decade, only few researches was established by Munding *et al.*, Missaggia *et al.*, Pfahler *et al.* and Harley *et al* [69-72]. Precipitously, microchannels in various applications were exploited throughout 1990s [73-88]. However, major efforts on microscale heat transfer studies were undertaken by the advent of twenty-first century [89-91]. Vigilent fluid flow and heat transfer phenomenon had improved the heat dissipation capacity in microchannel. In some researches, the definition of microchannel were confined based on convective confinement number and hydraulic diameter of the channels [83] [89] [92-94]. Extensive researches were reported for single phase fluid flow, multiphase fluid flow and boiling flow heat transfer in microchannels which extended microchannels as a promising candidate for cooling devices.

Foremost, the review of optimal design in microchannels was given by Goodling and Knight [95]. However, the evolution of microchannel passages was first addressed by Sobhan and Garimella [96]. Thermohydraulic performance of such passages was successfully fabricated and studied. Numerous techniques were explored concerning the geometry of microchannels marching for maximizing the heat transfer performance. Tullius *et al.* summarized the different enhancement techniques in microchannel with single-phase and two-phase laminar flow to improve its thermal performance [97]. Surface modifications by introducing micro-fins, adding grooves,

surface roughness, re-entrants, etc were discussed. Adham *et al.* presented a comprehensive review on rectangular microchannels in context to the influence of channel geometries, flow conditions, coolants used and microchannel material on fluid flow and heat transfer in the channels [98]. The gradual transition in analysis methods from experimental approach to analytical approach and later the excess dependence on numerical simulations and evolutionary algorithms for optimizations.

However, recent reviews were concerned on the thermo-hydraulic performance of different microchannels. Satish Kandlikar elaborated the single-phase and two-phase flow boiling processes and mechanisms in microchannel heat exchangers [99]. Methods to enhance the heat transfer performance and practical implication of flow boiling in microchannel heat exchangers were addressed. Dey *et al.* abridged the experimental observations and theoretical predictions through a thorough review on fluid flow and heat transfer characteristics of single-phase liquid flows through microchannels [100]. The deviation of transport characteristics in microscale was attributed to the geometrical, topographical and chemical features of microchannel substrate which was found to be not addressed by conventional theories. Asadi *et al.* presented a review of single-phase and two-phase microchannels [101]. The influence of channel geometries and flow regimes on pressure drop and heat transfer characteristics were extracted from the literature. Review also observed the paradigm shift in importance of numerical simulations and theoretical correlations for accurate experimental predictions. As reported, the experimental results were either over-predicted or under-predicted due to negligence of fluid behaviour in turbulent region. Kadam and Kumar summarized the experimental studies on pressure drop, heat transfer characteristics and flow pattern visualization in microchannel heat sink [102]. The importance given to parameters such as hydraulic diameter, saturation

temperature, mass flux, vapor quality, different coolants, channel geometry and number of channels were discussed and recommended the consideration of suitable influential parameters for further improvements. The hydrodynamic characteristics and the effect of critical heat flux on heat transfer coefficient were also discussed [103].

Meanwhile, innovative researches in modifying the microchannel cross-section and geometry for enhanced fluid flow are being conducted. The influence of geometry on the thermo-hydraulic performance in microchannels is primarily concentrated in this research while deserting the researches on heat transfer enhancement through nanofluids. Since the MCHS for LED applications are being implemented foremost, only single-phase heat transfer in microchannels are focussed in this thesis.

2.4 Selection of Microchannel

2.4.1 Microchannel with different cross-sections

In this section, the key studies on microchannels with different cross-section which appears in literature in the last decade as shown in Figure 2.6 are elaborated. Rectangular, circular, triangular, trapezoidal, elliptical, parabola and comparisons among microchannels with non-circular cross-sections are summarized.

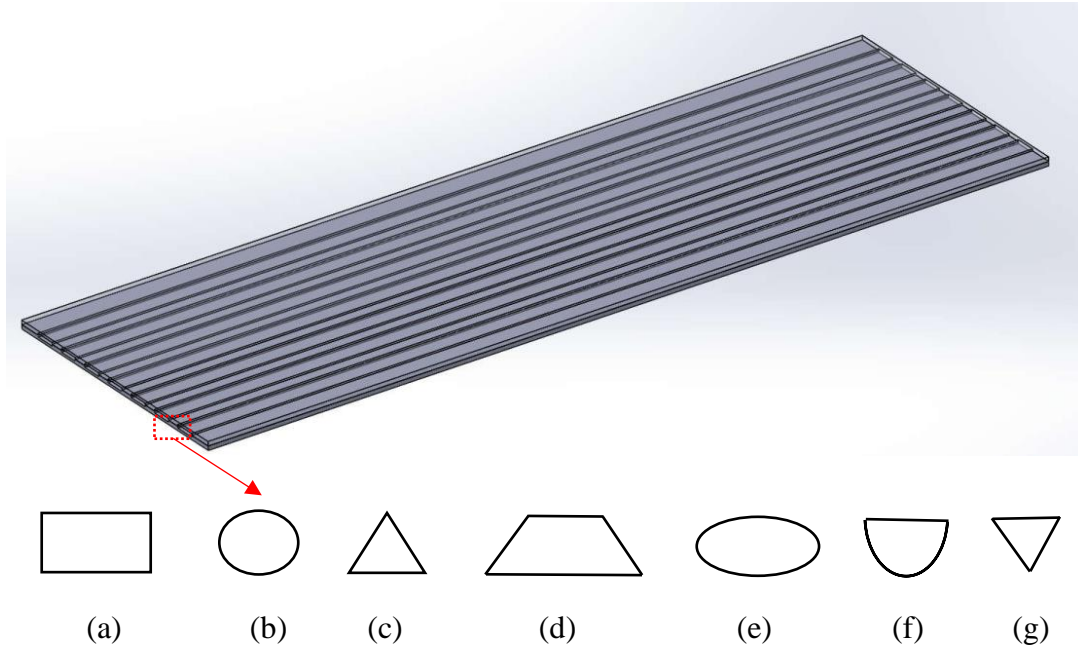


Figure 2.6: Parallel microchannel with different cross-sections (a) rectangular, (b) circular, (c)triangular, (d) trapezoidal, (e) elliptical, (f) parabolic and (g) V-shaped

2.4.1(a) Rectangular Microchannels:

Qu and Mudawar conducted comprehensive investigations on single phase rectangular MCHS to measure the pressure drop and heat transfer characteristics [104]. It was found that flow transition from laminar to turbulent was never observed in the proposed study. Pressure drop increased with increase in Reynolds number as the viscosity of fluid changes with temperature. However, higher heat transfer coefficient was observed with increase in Reynolds number. Chong *et al.* employed thermal resistance network model and CFD simulations to analyze thermal and hydrodynamic performance of Single-layer (SLCF) and double-layer (DLCF) counter flow microchannel [105]. The pressure drop, maximum surface temperature and thermal resistance of SLCF in laminar conditions were 122.4 kPa, 310K and 0.048K/W respectively whereas for DLCF the values were even lower. Li and Peterson conducted a detailed 3D numerical investigation for heat transfer to optimize the geometric structure in Silicon-based microchannel heat sinks [106]. Jung and

Kwak measured the convective heat transfer coefficients and friction factors of rectangular microchannels with water as working fluid [107].

The geometrical parameters influence the fluid flow and heat transfer characteristics of rectangular microchannels. Singh *et al.* primarily evaluated the impact of aspect ratio of rectangular microchannels on overall pressure drop during water boiling [108]. Pressure drop was found to be minimal at aspect ratio of 1.56 which was due to variation in frictional and acceleration pressure drops. Akbari *et al.* investigated the PDMS rectangular microchannels with pressure driven liquid flow to estimate pressure drop in arbitrary cross-section [109]. For the range of Reynolds number considered, the Poiseuille number were found to be a function of microchannel geometry and critical analysis on aspect ratio was a mandate for optimal pressure drop. Ambattipudi and Rahman numerically examined the effect of channel aspect ratio, number of channels and Reynolds number on conjugate heat transfer in silicon rectangular microchannels [110]. It was observed that Nusselt number decreases along the length of channel due to disruption in thermal boundary layers. Cao and Chen developed water-cooled rectangular microchannel heat sink for high power laser mirror to analyze the influence of microchannel geometry and operation parameters [111]. The effect of channel width, channel depth, fin width, mirror thickness and cooling domain on the performance of heat sink were analyzed. Conti *et al.* studied transient conjugate heat transfer by employing time-dependent heat flux on rectangular microchannels [112]. The effect of amplitude of heat flux variation, inlet velocity, geometry and thickness of heat sink were studied.

For wide range of heat flux, the channels with smaller width were found to be sensitive. Smith and Nochetto numerically simulated thermally developing laminar flow in rectangular microchannels with different aspect ratios (1 to 100) [113].

Consecutively, Park and Punch experimentally and numerically evaluated the friction factors and Nusselt number for laminar flow ($Re=69-800$) in rectangular microchannel with hydraulic diameter ranging from $106\ \mu\text{m}$ to $307\ \mu\text{m}$ [114]. Measured Friction factors agreed with the conventional theory for fully-developed flow. Mokrani *et al.* investigated the design and instrumentation of rectangular microchannel to depict the flow and convective heat transfer [115]. The influence of hydraulic diameter ($100\ \mu\text{m}$ to 1mm) was also studied. Sahar *et al.* discussed the effect of aspect ratio and hydraulic diameter on single phase flow rectangular microchannel [116]. Numerical simulations were performed for hydraulic diameters ranging from $0.1-1\ \text{mm}$ and aspect ratio ranging from $0.39-10$.

Kumaraguruparan and Sornakumar conducted experiments on aluminium microchannel heat sinks for different mass flow rate and heat input [117]. Nusselt number increased with increase in mass flow rate and heat input whereas the pressure drop increases with increased flow rate but decreases with increased heat input. The thermal resistance of the heat sink recorded to decrease with increase in pumping power and decreased with heat input. Tran *et al.* conducted numerical and experimental studies on Aluminium rectangular microchannel heat sink (hydraulic diameter = $296\ \mu\text{m}$) to investigate its pressure drop and performance index [118]. A high-performance index of $10.7\ \text{W/kPa}$ were recorded for highest mass flow rate.

2.4.1(b) Circular Microchannels:

Adams *et al.* conducted single phase forced convection experiments on circular microchannels with 0.6 and 1.09mm diameters. Nusselt number increases with decrease in channel diameter and increase in Re [119]. Further experiments were conducted with different channel diameters of 1.7 , 1.2 and 0.8mm [120]. In laminar

regime, the heat transfer coefficients were almost same independent of channel diameters. The transition of laminar to turbulent flow was smoother than expected. The influence of geometrical parameters such as different length and wall thickness on conjugate heat transfer in circular microchannels were studied by Nonino *et al* [121]. Considerable increase in axial heat conduction was observed for different wall thickness of circular microchannels. However, heat transfer enhancement for is limited in circular microchannels which serves as setback in electronics cooling applications.

2.4.1(c) Triangular Microchannels:

Research in microchannel with triangular cross-sections were begun by Niklas and Favle-Marinet [122]. They focused on split geometric effect from possible effects of hydrodynamics in parallel microchannels with triangular cross-section of hydraulic diameter 110 μm . Distinct research on triangular microchannel was carried out by Liao *et. al* [123]. Further, Xia *et. al* presented the numerical simulation on water and heat transfer characteristics in microchannel heat sink with triangular reentrant cavities [124]. The thermal boundary layer along constant cross section enhanced the heat transfer performance with the improved Reynolds number. Kuppusamy *et. al* suggested the highest thermal performance can be achieved in triangular micromixer (MTM) without additional pressure drop by appropriate flow rate, micro mixer angle and size of microchannel heat sink for constant volumetric flow rate of $9 \times 10^{-7} \text{ m}^3/\text{s}$ [125]. In another way, they found that highest thermal enhancement can be attained by reducing the outer angle and increment of the inner angle and in number of micro mixer with significant reduction in pressure loss.

2.4.1(d) Trapezoidal Microchannels:

Over last decade, Wu and Cheng were the first to investigate the influence of geometrical parameters on laminar convective heat transfer and pressure drop in silicon trapezoidal microchannels [126]. Friction constant and Nusselt number increased with increase in surface roughness and hydrophilic property and prone to increase more with Reynolds number. Niazmand *et al.* numerically investigated the velocity and temperature fields in slip-flow regime of trapezoidal microchannels by control-volume based numerical method [127]. Microchannels with aspect ratio (0.25-2), side angles (30°-60°) were considered and subjected to Reynolds number (0.1-10) and constant wall temperature. Friction and heat transfer coefficients were observed to reduce at the entrance region due to high velocity-slip and temperature-jump. Geometrical optimizations using response surface methodology and numerical study were carried out to minimize the thermal resistance of heat sink. [128] [129]. The effects of width, depth, fin width aspect ratio and thermo-hydraulic wall interaction were explored.

Estimation of hydraulic diameter in trapezoidal microchannel had remained debatable over the years. Sadeghi *et al.* proposed a method to calculate the characteristic length of trapezoidal microchannel to evaluate the Nusselt number [130]. The proposed model was a function of geometrical parameters such as area, perimeter and polar moment of inertia. Chai *et al.* experimentally verified the laminar flow and heat transfer in silicon trapezoidal microchannel [131]. For constant pumping power, thermal resistance decreased with increase in heating power while the sub-thermal resistance remained unchanged at 7.5%. However, the sub-thermal resistance increased initially and approached to an asymptote of 0.79 for increased pumping power. Recently, Khan *et al.* optimized the microchannels with inverse trapezoidal

cross-section by numerical investigation and multi-objective evolutionary algorithm [132]. Optimization of three design variables: width, depth and angle of the channel were studied to lower thermal resistance and pressure drop.

2.4.1(e) Non-circular Microchannels:

Apart from extensive examinations on individual cross-section, the non-circular cross-sections were compared by many researchers. Numerous researches were performed to analyze the influence of non-circular cross-sections on pressure drop and friction factor in microchannels [133-136]. The friction factor was found to vary with change in hydraulic diameters of different cross-sections. Rectangular microchannels had reduced effect on friction factor while the triangular channels had significant effect on microchannels [133]. Microchannels with small hydraulic diameter lead to higher heat transfer coefficients and low pressure drop. Additionally, the friction factor decreased nonlinearly with increase in Reynolds number due to viscous forces on the walls [134]. Hydraulic diameter, aspect ratio and solid volume fraction were optimized for minimization of wall temperature and pressure drop [135]. In general, rectangular microchannels holds high heat transfer coefficient and low thermal resistance followed by trapezoidal and triangular cross-sections.

2.4.1(f) Microchannels with unique cross-sections:

Duan and Muzychka predicted the Poiseuille number for slip flow in elliptical microchannels [137]. Po increases with increase in Kn for constant aspect ratio and when aspect ratio becomes 1, the elliptical channels transforms as circular tubes. Vocale *et al.* numerically investigated the fully developed gas flow through elliptical microchannel [138]. Microchannels with different heated perimeter lengths, wetted perimeter and aspect ratio were considered. Few theoretical examinations on parabolic

microchannels were studied and unfortunately, it has not been considered for extensive research due to complexity in manufacturing [139] [140]. Peng et. al investigated flow boiling of water and methanol through V-shape microchannels and its effect on heat transfer characteristics [141]. Liquid flow fluctuations occur at high heat flux lead and blocks the inlet enabling large bubble formation. Besides, heat transfer coefficient and pressure drop in microchannel were affected by increase in liquid flow velocity. Groove angle of V-shape also affected the heat transfer and the fluid flow via microchannel. Efficiency of V-shaped microchannel was recorded higher than the conventional heat dissipating devices with temperature difference of 11.85 K and area heat resistance of $0.0237 \text{ K.cm}^2/\text{W}$ [142].